Journal of Volcanology and Geothermal Research 392 (2020) 106767

Contents lists available at ScienceDirect

Journal of Volcanology and Geothermal Research

journal homepage: www.elsevier.com/locate/jvolgeores

Volcanic conduit controls on effusive-explosive transitions and the 2010 eruption of Merapi Volcano (Indonesia)

Brett B. Carr [a,b,*], Amanda B. Clarke [b,c], Mattia de' Michieli Vitturi [c,d]

[a] Lamont-Doherty Earth Observatory, Columbia University, Palisades, NY, USA
[b] School of Earth and Space Exploration, Arizona State University, Tempe, AZ, USA
[c] Instituto Nazionale di Geofisica e Vulcanologia, Sezione di Pisa, Italy
[d] Department of Geology, University at Buffalo, Buffalo, USA

ARTICLE INFO

Article history:
Received 21 February 2019
Received in revised form 16 December 2019
Accepted 27 December 2019
Available online 07 January 2020

Keywords:
Merapi
Explosive-effusive transitions
Eruption rate
Fragmentation
Lava domes
Explosive eruptions

ABSTRACT

Individual volcanoes can produce both effusive and explosive eruptions. A transition between these two eruption styles dramatically changes the hazards and can occur either between distinct eruption events or within one eruption episode. The causes of these transitions are difficult to determine due to the number of system parameters that can influence whether or not magma fragments in a runaway process. We apply a numerical model of magma ascent in a volcanic conduit to isolate and test the effects of key parameters related to magma rheology and system geometry. We find that for a given volcanic system, parameters that control magma viscosity, such as initial water mass fraction, initial crystal volume fraction, and temperature, have the greatest influence on whether or not magma fragments during ascent and erupts explosively. We also define a 'critical condition' for the full set of initial parameters under which a transition in eruption style, from effusive to explosive or the reverse, is more likely to occur. Under these conditions, small heterogeneities in the water or crystal content of the magma, or small perturbations to the conduit pressure gradient due to magma chamber overpressure or dome growth or collapse, can disrupt the magmatic conditions and cause a transition in eruption style. The 2010 VEI 4 eruption of Merapi Volcano included both effusive and explosive phases and was larger by an order of magnitude than its eruptions during the previous century. We constrain our model for the Merapi system using published literature values and show that between the previous eruption in 2006 and the 2010 eruption, the shallow magmatic system at Merapi reached critical conditions due to the ascent from depth of a large, hotter, more volatile-rich magma. Under these critical conditions and according to our model results, small changes in the volatile content of the magma, small dome collapses, subtle changes in degassing rate, or the addition of CO_2 to the magma through decarbonation of the bedrock, are all feasible mechanisms for triggering rapid transitions between effusive and explosive activity during the 2010 eruption period.

1. Introduction

Volcanic eruptions, whether effusive or explosive, have significant impacts on their surroundings. While explosive eruptions are more violent and their hazards more far-reaching, effusive eruptions can persist for decades and pose a continuous long-lived hazard (Simkin, 1993; Wolpert et al., 2016). Transitions between eruptive styles can compound hazards, as deviations from a "typical" eruption at a volcano can catch the local population unprepared for a larger or longer-lasting event. Persistently active volcanoes are especially hazardous in this sense, as long stretches of "typical" or background activity can create a dangerous false sense of security. Numerical modeling is a useful technique to test the conditions leading to eruptions of varying size (Mastin, 2002). Constraining a model to simulate the conditions of an active or potentially active system can help understand the range of possible behaviors and the potential for transitions in eruptive style (Wilson et al., 1980). Here, we apply a numerical model of magma ascent in a volcanic conduit to show the effect of chamber pressure and different magmatic and geometric properties on eruption style and then apply the model to explain the variations in explosive and effusive activity during the 2010 eruption of Merapi Volcano.

1.1. Transitions between explosive and effusive activity

An explosive eruption is initiated by fragmentation of the magma. Fragmentation is a runaway process of brittle failure of the remaining melt phase of the magma mixture which can occur when the volume fraction of the exsolved volatile phase is sufficiently large (Sparks,

* Corresponding author at: School of Earth and Space Exploration, Arizona State University, Tempe, AZ, USA.
E-mail address: bcarr@ldeo.columbia.edu (B.B. Carr).

https://doi.org/10.1016/j.jvolgeores.2019.106767
0377-0273/

1978; Woods and Koyaguchi, 1994), the strain rate in the rapidly ascending magma is sufficiently high (Papale, 1999; Gonnermann and Manga, 2003), or bubble overpressure exceeds a critical value (Zhang, 1999). These conditions lead to a dramatic transition, from a state in which a liquid-solid magma phase (the carrier or continuous phase) contains and transports exsolved volatiles, to a gas-driven mixture in which the expanding gas carries particles of melt and crystals.

Previous works have discussed controls on eruption style (i.e. whether or not the magma fragments) in terms of increasing pressure in a magmatic system and the ability of that system to dissipate the pressure through degassing (Woods and Koyaguchi, 1994; Ruprecht and Bachmann, 2010; Kozono and Koyaguchi, 2012). As additional pressure in the system drives an increase in ascent rate, proportionally less gas is able to escape the system in an open-system manner and the magma density decreases. The lower density causes the magma to rise faster and potentially 1) reach the maximum bubble volume fraction as volatiles exsolve during ascent and cannot escape the system; 2) exceed the critical strain rate value due to rapid ascent; and/or 3) reach the surface with an overpressured bubble phase; all conditions resulting in fragmentation causing an explosive eruption (Woods and Koyaguchi, 1994; Papale, 1999; Zhang, 1999; Melnik and Sparks, 2002). Woods and Koyaguchi (1994) suggest that overpressure in the conduit system can be generated if supply rate from depth is greater than the mass flow rate at the vent, and transitions between effusive and explosive eruptions occur to relieve this overpressure.

Transitions in eruption style can also be affected by near-surface processes. Lateral degassing through the conduit walls promotes effusive eruptions by removing gas from the magma and preventing the critical bubble volume fraction from being reached (Jaupart and Allègre, 1991). Variations in the permeability of the conduit wall rock, which controls the rate of lateral degassing, can thus lead to different types of eruptions (Woods and Koyaguchi, 1994; Diller et al., 2006; Clarke et al., 2007; Kozono and Koyaguchi, 2012; Degruyter et al., 2012). Lava domes can also have significant impact (Woods and Koyaguchi, 1994; Melnik and Sparks, 1999). Dome growth can suppress fragmentation by increasing the pressure at the vent, which reduces the pressure gradient driving ascent. Conversely, dome collapse can relieve confining pressure and trigger explosive eruptions (Woods and Koyaguchi, 1994; Melnik and Sparks, 1999). Melnik and Sparks (1999) also model how small changes in dome height can significantly vary the mass flow rate and show that the effects can be similar for minor variations in magma chamber overpressure and magma volatile content.

Magma viscosity strongly affects the potential for magma fragmentation. Kozono and Koyaguchi (2012) describe a feedback mechanism whereby higher flow rates result in less crystallization during ascent and thus lower viscosities which promote further increases in flow rate. However, Ruprecht and Bachmann (2010) show that pre-eruptive heating of a silicic magma chamber by mixing with a recharge batch of magma can promote effusive eruptions by lowering viscosity and allowing more efficient gas loss from a permeable system.

Many of the factors described here cause nonlinear changes (Melnik and Sparks, 1999; Kozono and Koyaguchi, 2012; Degruyter et al., 2012), such that small changes in certain variables can result in large changes in mass flow rate and potentially in effusive-explosive transitions.

1.2. Recent Merapi activity

Merapi Volcano is located in central Java (Fig. 1) and for millennia has been one of Indonesia's deadliest and most active volcanoes (Newhall et al., 2000; Voight et al., 2000). During the 20th and early 21st centuries Merapi was consistently active, with a nearly continuous effusive eruption constructing a series of lava domes at the vent (Voight et al., 2000). Effusive activity was characterized by long periods of very slow extrusion rate (< 0.1 m^3 s^{-1}) interrupted every few years by short episodes of elevated extrusion rates (1–4 m^3 s^{-1}) lasting weeks to months (Siswowidjoyo et al., 1995). The periods of elevated extrusion rate were accompanied by dome collapse-generated block-and-ash flows, which caused a majority of the casualties and damage associated with the eruptions. This pattern of activity was so persistent for over 100 years that it became known as "Merapi-type" activity and eruptions at other volcanoes are described using this term (Voight et al., 2000). The most recent "Merapi-type" eruption at Merapi occurred in May–July 2006 (Ratdomopurbo et al., 2013).

The 2010 eruption at Merapi broke the recent pattern in dramatic fashion. On October 26, 2010, following a period of intense precursory signals, an explosive eruption destroyed the 2006 lava dome and generated an ash plume that reached 12 km altitude (Surono et al., 2012). Following this explosion, rapid lava extrusion in excess of 25 m^3 s^{-1} built a new lava dome (Pallister et al., 2013). After this period of rapid lava extrusion, the climactic explosion occurred on 4–5 November and was classified as VEI 4 (Volcano Explosivity Index; Newhall and Self, 1982) with an eruption plume reaching an altitude of 17 km (Pallister et al., 2013). Based on plume heights and the models of Wilson and Walker (1987) and Mastin et al. (2009), we estimate mass flow rates during the explosive phases of the eruption to have been on the order of 10^6–10^7 kg s^{-1}. During the waning phase of the eruption a new dome was emplaced at a rate of 35 m^3 s^{-1} (Pallister et al., 2013). Extrusion rates during the 2010 eruption were an order of magnitude greater than extrusion rates during the 2006 and previous 20th century effusive eruptions (Ratdomopurbo et al., 2013; Hammer et al., 2000). Column-collapse pyroclastic density currents (PDCs) reached up to 16 km from

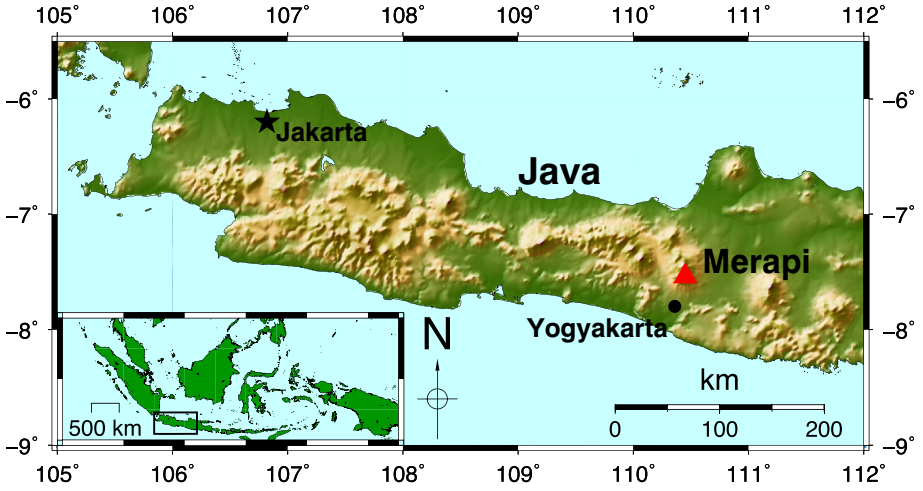

Fig. 1. Location of Merapi Volcano. Merapi (triangle) is located in central Java, 30 km north of the city of Yogyakarta. Inset: Location of the main map (box) within the Indonesia archipelago.

the vent during the November 4–5 explosion, compared to 7 km for the largest dome-collapse PDCs from the 2006 eruption (Charbonnier and Gertisser, 2008; Charbonnier et al., 2013). As a result of the significant increase in eruption intensity in 2010, 367 people were killed by pyroclastic flows and surges - the deadliest eruption at Merapi since 1931 (Voight et al., 2000; Surono et al., 2012). The previous VEI 4 eruption at Merapi occurred in 1872, and eruptions of this size were more common in the two millennia prior to that year compared to the past 150 years (Voight et al., 2000; Newhall et al., 2000; Gertisser et al., 2012).

Surono et al. (2012), Costa et al. (2013), and Preece et al. (2016) suggest the exceptional size of the 2010 eruption was caused by the rapid ascent of an unusually large and volatile-rich batch of magma from depth, although the exact mechanisms suggested by the groups vary in detail. This magma had similar composition to the 2006 magma (Costa et al., 2013), but the size and ascent rate overwhelmed the capacity of the shallow, crystal-rich storage system at Merapi that had slowed previous rising magma batches, allowing them to degas and erupt effusively (Costa et al., 2013). Costa et al. (2013) also discuss the potential impact of crustal carbonate assimilation on the 2010 eruption, as this process likely played an important role during the 2006 Merapi eruption (Troll et al., 2012; Carr et al., 2018). For 2010, the addition of CO_2 via decarbonation likely contributed to the exceptionally high ascent rates and explosivity, though the importance of this contribution relative to other factors is unclear (Costa et al., 2013). Surono et al. (2012) attribute the explosivity of the 2010 eruption to the separation of a gas phase from the magma that ascended rapidly to the surface, while they attribute the alternation between effusive and explosive eruption phases to variable volatile content in the magma. Preece et al. (2016) attribute the effusive-explosive transitions to variations between open- and closed-system degassing that occurred as a result of degassing and crystallization feedback mechanisms in the shallow conduit.

2. Methods

We use a numerical model for magma ascent in a vertical conduit based on the theory of thermodynamically compatible systems (Romenski et al., 2010; de' Michieli Vitturi et al., 2011; La Spina et al., 2015; La Spina et al., 2017). The model is 1D, two-phase, multicomponent, and steady-state, as in Carr et al. (2018), and includes the key processes that control magma ascent dynamics, such as degassing and crystallization and associated rheological changes, magma fragmentation, and viscous interaction with conduit walls. Here, we assume isothermal conditions, a reasonable assumption for a long-lived, well-insulated plumbing system (La Spina et al., 2017). The model is an extension of that for basaltic systems by La Spina et al. (2015), such that we add lateral degassing, assume only one crystal phase, and use a basaltic andesite bulk composition with a rhyolitic melt phase (based on whole rock and glass composition measurements by Hammer et al., 2000 and Innocenti et al., 2013).

As magma rises, exsolution of volatiles and crystallization change the density and viscosity of the melt (Hess and Dingwell, 1996). The evolving viscosity of the magma mixture is represented by a function with three components (eq. 5, Carr et al., 2018): 1) the bubble-free, crystal-free liquid (melt) viscosity, which is a function of the temperature and dissolved water content (eq. 7, Hess and Dingwell, 1996); 2) an increase in magma viscosity due to the presence of crystals, calculated using a non-dimensional factor (eq. 9, Costa, 2005); and 3) a change in magma viscosity due to the presence of bubbles, accounted for by another non-dimensional factor (eq. 7, Llewellin and Manga, 2005). Lateral degassing occurs when conduit overpressure is greater than lithostatic pressure and exsolved gas volume fraction reaches a threshold value of 60%, deemed sufficient to allow permeable connectivity (Eichelberger et al., 1986). We use the rate of lateral degassing as defined by Jaupart and Allègre (1991) and a value for wall rock permeability of 4.8×10^{-14} m^2 as in Diller et al. (2006) and Clarke et al. (2007). For a full description of the model and its governing equations, the reader is referred to Carr et al. (2018).

We use a critical bubble volume fraction to define the fragmentation threshold. At this critical value the bubble volume fraction is too large for the melt phase to remain connected and magma fragmentation occurs. Previous works have applied a strain-rate (Papale, 1999) or bubble-overpressure (Zhang, 1999) fragmentation criteria. Comparison of the effects of different fragmentation criteria on the results of numerical conduit models showed that the temporal evolution of fragmentation- whether steady or pulsating- depended on the criteria used (Melnik and Sparks, 2002). However, properties at the initiation of fragmentation and resulting vent velocity and mass flow rate- the quantities we are most interested in for this study- have been shown to be similar to first order for different fragmentation criteria in multiple conduit models (Melnik and Sparks, 2002). This result can be explained: because of steep spatial gradients for all the variables immediately below the fragmentation level, where bubble volume fraction is high, ascent rates and strain-rates tend to also be high (Melnik and Sparks, 2002; Degruyter et al., 2012; La Spina et al., 2019). And thus, one critical value will be reached nearly simultaneously with the others. Because of this correlation among all criteria, we conclude that a critical bubble volume fraction is a reasonable fragmentation criterion for our applications discussed below. Following previous works (Woods and Koyaguchi, 1994; Kozono and Koyaguchi, 2012; Degruyter et al., 2012), we use a value of 0.8, above which the magma will fragment. We also tested values in the range of 0.7–0.8 and find that the trends in our results, as discussed later, are unchanged, although, as expected, explosive eruption is more likely to occur with a criterion of 0.7 (see Supplemental Figs. S1 and S2).

Below the fragmentation level, the liquid phase (a mixture of melt, crystals and dissolved volatiles) represents the continuous phase while the exsolved gas is the dispersed phase, and the drag force between the two phases is defined to retrieve the permeable outgassing Forchheimer's law (Degruyter et al., 2012). Above the fragmentation level, the exsolved gas constitutes the continuous phase while magma fragments constitute the dispersed phase, and the drag force between the two phases is modeled as in Degruyter et al. (2012) and La Spina et al. (2015).

We investigate the effects of different parameters on mass flow rate and magma fragmentation using the Dakota toolbox (Adams et al., 2014). Dakota is an open-source software developed at Sandia National Laboratories providing a flexible and extendable interface between analysis codes (in our case the conduit model) and iterative systems analysis methods. For our variable sensitivity analyses we conduct two types of runs. First, we hold all but one parameter constant to isolate individual effects. Second, we use sets of three free parameters and run the model for combinations of values for those three variables to investigate the relationship among parameters in a dynamic system. Dakota allows these sets of model runs to be conducted iteratively without manual manipulation of input values, dramatically streamlining the process. In total, the output of over 1500 model runs are included here.

We choose a set of model input values representative of previous research on multiple volcanic systems (standard values) to define two standard runs (one effusive and one explosive) to use during our variable sensitivity analysis (Table 1). We use a conduit length of 5000 m, conduit radius of 15 m, and temperature of 850 °C as in Melnik and Sparks (1999), Kozono and Koyaguchi (2012), and de' Michieli Vitturi et al. (2013). The pressure at the conduit inlet (magma chamber) is 130 MPa, which assumes lithostatic pressure with a country rock density of 2650 kg m^{-3}3^3. The pressure at the conduit outlet (vent) is ~3.6 MPa, based on a 150 m tall dome (Calder et al., 2002; Nakada et al., 1999; Ratdomopurbo et al., 2013) with a density of 2400 kg m^{-3} (Komorowski et al., 2013). Initial water mass fraction is 0.04 (Degruyter et al., 2012; Costa et al., 2013) and initial crystal volume fraction is 0.44 (effusive) and 0.22 (explosive) (Melnik and Sparks, 1999; Hammer et al., 2000; Degruyter et al., 2012).

Table 1
Input parameters. Parameter values used as input for the numerical model for the standard run and Merapi 2010 eruption phases. Run 1 = October 26 initial explosive phase. Run 2 = Effusive phase. Run 3 = Initiation of Nov 4–5 explosive phase- H_2O change. Run 4 = Initiation of Nov 4–5 explosive phase- dome height change. Run 5 = Initiation of Nov 4–5 explosive phase- wall-rock permeability change. Run 6 = Initiation of Nov 4–5 explosive phase- magma chamber overpressure change. Run 7 = Initiation of Nov 4–5 explosive phase- addition of crustal CO_2. Run 8 = Nov 4–5 explosive phase- low H_2O. Run 9 = Nov 4–5 explosive phase- higher H_2O. Values in bold (Runs 3–9) indicate values changed to cause fragmentation to occur compared to the values for the effusive Run 2.

	Units	Standard runs	Standard range	Merapi literature	Merapi 2010 eruption conditions								Merapi 2006[a]
					Run 1	Run 2	Run 3	Run 4	Run 5	Run 6	Run 7	Run 8	Run 9	
H_2O mass fraction		0.04	0.02–0.06	0.04–0.06[f]	0.04	0.04	**0.041**	0.04	0.04	0.04	0.04	0.04	**0.05**	0.025
Crystal volume fraction		0.44[d] 0.22[e]	0.2–0.6	0.3–0.5[g]	0.44	0.44	0.44	0.44	0.44	0.44	0.44	0.44	0.44	0.50
Temperature	°C	850	800–1000	950–1000[f]	970	970	970	970	970	970	970	970	970	950
Dome height	m	150	0–300	0–150[h]	50	130	130	**120**	130	120	120	**0**	**0**	250
Chamber overpressure	MPa	0	0–10		0	0	0	0	0	**3**	**6**	0	0	7
Wall-rock permeability	m^2	4.8×10^{-14}	4.8×10^{-11} –4.8×10^{-16}		4.8×10^{-14}	4.8×10^{-12}	4.8×10^{-12}	4.8×10^{-12}	**4.8×10^{-14}**	4.8×10^{-12}	4.8×10^{-12}	4.8×10^{-12}	4.8×10^{-12}	4.8×10^{-14}
Solubility coefficient		4.11×10^{-6}			4.11×10^{-6}	4.11×10^{-6}	4.11×10^{-6}	4.11×10^{-6}	4.11×10^{-6}	4.11×10^{-6}	**3.61×10^{-6}**[k]	4.11×10^{-6}	4.11×10^{-6}	3.31×10^{-6}
Conduit length	m	5000	1000–6000	1500–2500[i]	2000	2000	2000	2000	2000	2000	2000	2000	2000	2000
Conduit radius	m	15	10–30		15	15	15	15	15	15	15	15	15	15
Volume flow rate[b]	$m^3\ s^{-1}$	2.2[d]		25–35[h]		28.1								3.5
Mass flow rate[c]	$kg\ s^{-1}$	3.1×10^5		10^6–10^7[j]	1.4×10^6		1.6×10^5	1.9×10^5	1.72×10^5	2.1×10^5	2.0×10^5	3.7×10^6	5.3×10^6	
Eruption style					Explosive	Effusive	Explosive	Explosive	Explosive	Explosive	Explosive	Explosive	Explosive	Effusive

[a] Peak eruption phase, from Carr et al. (2018); [b] For effusive eruptions; [c] For explosive eruptions; [d] Standard Effusive Run, Fig. 2a; [e] Standard Explosive Run, Fig. 2b; [f] Costa et al., 2013; [g] Hammer et al., 2000; [h] Pallister et al., 2013; [i] Ratdomopurbo and Poupinet, 2000; [j] Wilson and Walker (1987) & Mastin et al. (2009), based on plume heights of 12–17 km reported by Pallister et al. (2013); [k] Decrease in solubility coefficient corresponds to the addition of 4000 ppm CO_2 (Papale et al., 2006).

The model sensitivity to each variable was then evaluated over a range of 0.02–0.06 for initial water mass fraction, 0.2–0.6 for initial crystal volume fraction, 800–1000 °C for the temperature, −11 to −16 for the lateral permeability exponent, 10–30 m for the conduit radius, 1000–6000 m for the conduit length, 0–300 m for the dome height, and 0–10 MPa for the magma chamber overpressure. These standard ranges were chosen based on values used in previous works addressing a number of different volcanic systems (Jaupart and Allègre, 1991; Melnik and Sparks, 1999; Voight and Davis, 2000; Hammer et al., 2000; Degruyter et al., 2012; de' Michieli Vitturi et al., 2013; Costa et al., 2013).

3. Results

3.1. Reference Runs

The model output for the standard runs is shown in Fig. 2. We note the strong effect of lateral open-system degassing for the standard effusive run, which initiates when the bubble volume fraction equals 0.6 near the top of the conduit (dashed line, Fig. 2a). Significant lateral degassing causes decreases in the mass flow rate, the velocity of both phases, and the bubble volume fraction above the degassing initiation point. Decreasing the initial crystal volume fraction by a factor of two (from 0.44 to 0.22) results in an explosive eruption (Standard Explosive Run, Fig. 2b) with fragmentation occurring ~1000 m below the vent (dashed line, Fig. 2b). In this case, because of the lowered magma viscosity, the ascent rate is too high relative to the rate of lateral degassing, such that gas loss through the conduit walls cannot suppress fragmentation, resulting in an explosive eruption (Fig. 2b).

We individually vary eight parameters over their standard range to show the effect of each parameter on the mass flow rate (Fig. 3). For three variables (initial crystal volume fraction, temperature, and dome height), the standard range of values (Table 1) includes a transition between explosive and effusive activity (stars, Fig. 3). Of the parameters controlling magma viscosity – crystal volume fraction, temperature, and water mass fraction – no single parameter appears to exert more control on fragmentation compared to the others. For the standard effusive run (Fig. 2a; Fig. 3), the initial crystal volume fraction and temperature dominate the viscous effects such that increasing initial water mass fraction from the standard value (Table 1) cannot induce fragmentation (Fig. 3a). This result occurs because our standard values for initial crystal volume fraction (0.44) and temperature (850 °C) strongly favor high viscosities and effusive eruptions. Similarly, when initial water mass fraction is fixed at a value of 0.02 (half the standard value of 0.04) and the other parameters are varied, water content dominates the result and prevents fragmentation (compare slope of blue line (0.02) to that of the red line (0.04), Fig. 3b).

Parameters related to system geometry or pressure, such as conduit radius, conduit length, magma chamber overpressure, and dome height (Fig. 3e, f, g, h), have variable effect on mass flow rate and do not exert significant control on eruption style for the ranges shown. Conduit radius (Fig. 3e) causes a variation in mass flow rate that is of similar magnitude to that caused by changes in initial crystal volume fraction (Fig. 3b) or temperature (Fig. 3c), but unlike those two parameters, changes in conduit radius over this range do not lead to a change in eruption style. Within the effusive regime, dome height has a relatively small effect on mass flow rate (Fig. 3g). However, dome height has a strong control on eruption style, as below a certain dome height, the confining pressure at the vent is sufficiently low to allow fragmentation (Fig. 3g). For the set of input parameters chosen for our standard effusive run, wall rock permeability has little to no effect on mass flow rate (Fig. 3d).

The initial viscosity of magma leading to effusive eruptions is generally higher than that for explosive runs (Fig. 4a). Viscosity increases during ascent for both types of runs as volatiles exsolve from the melt. The lower viscosity for the explosive run (due solely to a reduced initial

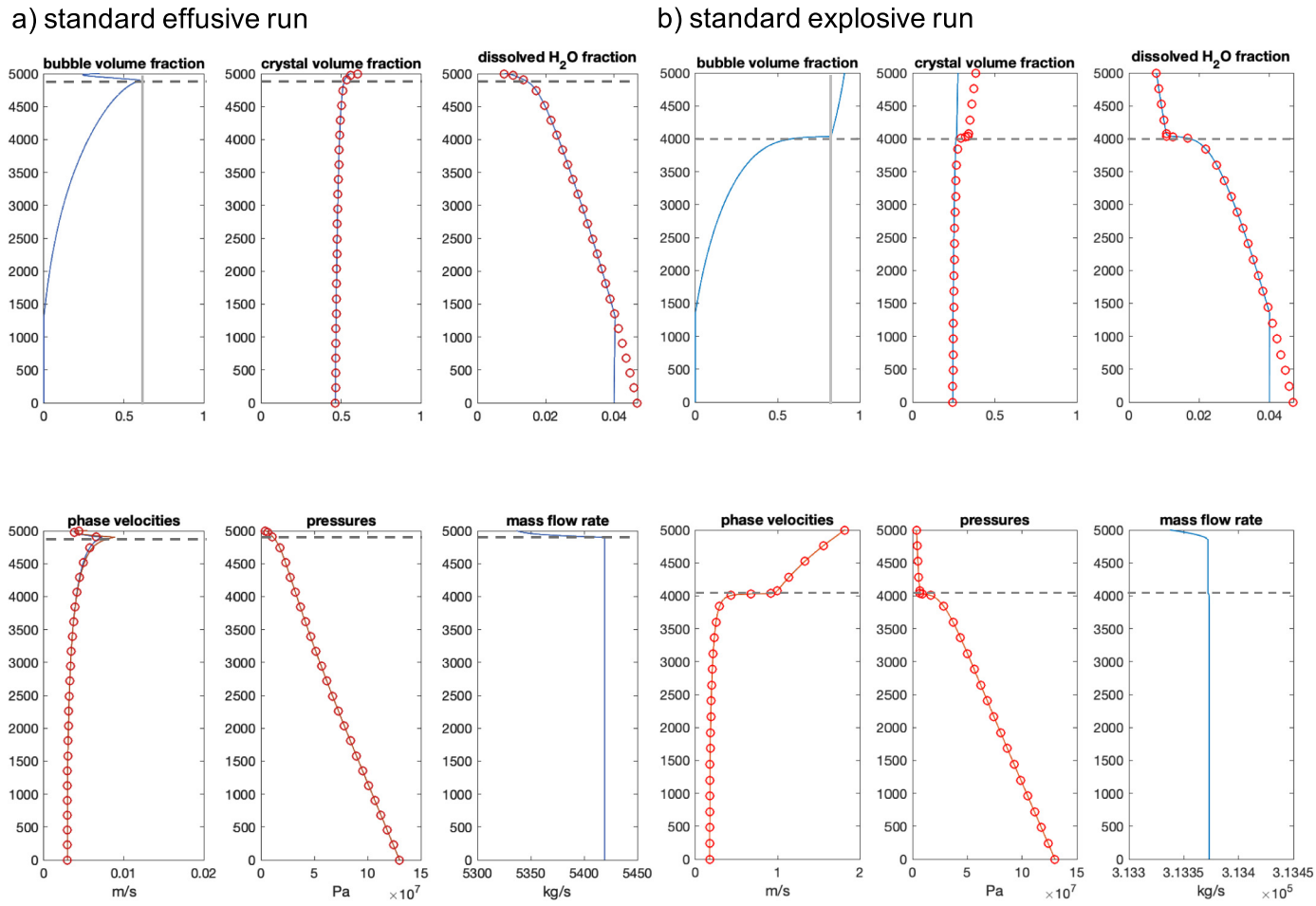

Fig. 2. Model results for magma ascent. Each panel shows the ascent conditions for six different parameters for our standard effusive run (a) and standard explosive run (b) where the initial crystal volume fraction was reduced by a factor of two. The y-axis is distance in meters along the conduit from the magma chamber to the vent. Solid blue lines are the values for the melt phase during ascent. Solid red lines are for the bubble phase. Open circles are equilibrium conditions for a given value at that location in the conduit. Where the solid blue line deviates from equilibrium near the vent for the crystal volume fraction in (b), ascent is too rapid for the rate of crystallization to keep up with depressurization. Horizontal dashed lines show the depth of lateral degassing initiation (a) and the fragmentation level (b). Thin vertical line in the bubble volume fraction panel (top left) show that (a) lateral degassing initiates at bubble volume fraction = 0.6 and (b) fragmentation occurs when bubble volume fraction = 0.8. (For interpretation of the references to colour in this figure legend, the reader is referred to the web version of this article.)

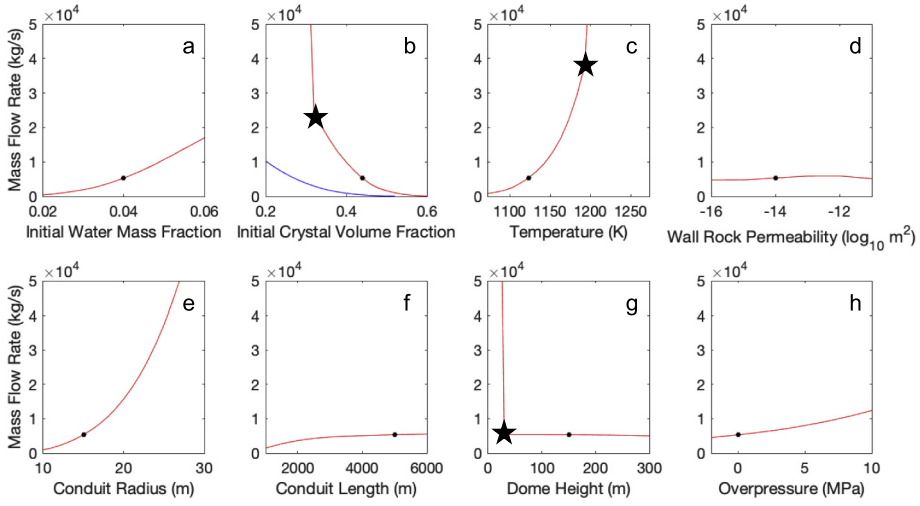

Fig. 3. Variable effects on mass flow rate. Different parameters have different effects on the mass flow rate, shown here with each panel representing variation in one parameter while the others are held constant at the standard values. Stars show where fragmentation occurs for initial crystal volume fraction (b), temperature (c), and dome height (g). The blue line in the initial crystal volume fraction panel (b) shows the mass flow rate for a reduced initial water mass fraction of 0.02, which prevents fragmentation. The black dot in each panel indicates the conditions for the standard effusive run (Table 1, Fig. 2a). (For interpretation of the references to colour in this figure legend, the reader is referred to the web version of this article.)

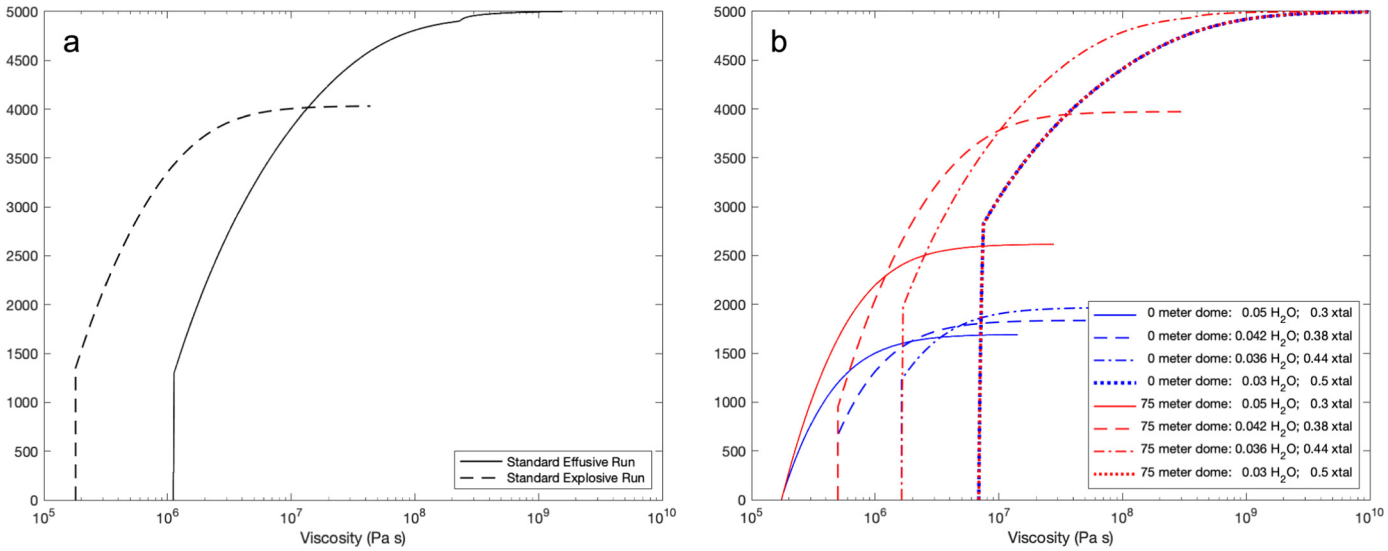

Fig. 4. Viscosity of magma during ascent. The viscosity of the magma during ascent is shown for the standard effusive and explosive runs (a) and for model runs representing a range of initial viscosities and two different dome heights (b). The y-axis is distance in meters along the conduit from the magma chamber to the vent. In (b), blue lines are runs with no dome at the vent and red lines are for a 75 m dome. The line pattern (solid, dashed, etc.) corresponds to the initial water and crystal contents of the magma, which control the initial viscosity. Effusive runs in both panels are identified by the line representing viscosity continuing to the vent (y-axis = 5000). The magma viscosity plotted here is valid only when the melt is the continuous phase and is therefore not plotted for explosive runs above the fragmentation level where the magma becomes a gas-driven mixture. Explosive runs generally have lower initial viscosity compared to effusive runs. For runs with the same initial viscosity, fragmentation is more likely when pressure at the vent is lower, which increases the pressure gradient. Lower viscosity and higher pressure gradient both lead to higher ascent rates, which makes fragmentation more likely during ascent. (For interpretation of the references to colour in this figure legend, the reader is referred to the web version of this article.)

crystal volume fraction in the case of Fig. 4a) leads to higher ascent rates and a more rapid increase of the bubble volume fraction (compare top left panel in Fig. 2a & b), causing the fragmentation threshold volume fraction of 0.8 to be reached during ascent. The pressure gradient between the conduit inlet at depth and the vent also controls the ascent rate such that runs with the same initial magma viscosity can be effusive with a 75 m dome at the vent (which reduces the pressure gradient and slows ascent) and explosive if vent pressure is atmospheric (compare red and blue lines, Fig. 4b). However, viscosity is the primary control for the runs with the highest initial viscosity (dotted lines, Fig. 4b), the viscosity controls the ascent rate such that ascent conditions are identical for no dome and a 75 m dome.

We also look at the relationships between multiple varying parameters and their relative effect on mass flow rate and fragmentation. For these sets of runs we focus on initial water mass fraction and initial crystal volume fraction over ranges of 0.03–0.05 and 0.3–0.5, respectively, and three different 'third' parameters - temperature (850 and 950 °C), dome height (0, 75, and 150 m), and magma chamber overpressure at the conduit inlet (0, 5, and 10 MPa). In the surface plots presented in Fig. 5, each surface represents a fixed value of the third parameter. The bottom surfaces are least likely to be explosive, while the top surfaces are most likely to be explosive. The influence of the third parameter on the mass flow rate, relative to the initial water mass fraction and initial crystal volume fraction, is shown by the spacing between surfaces such that temperature has a relatively large effect on mass flow rate (Fig. 5a, wide spacing) while overpressure does not (Fig. 5b, tight spacing). Initial water mass fraction, initial crystal volume fraction, and temperature all control the viscosity of the melt, so the combined effect of all three parameters, as they move towards values that decrease viscosity (from bottom right to top left in Fig. 5a), is a rapid increase in mass flow rate (2–3 orders of magnitude, Fig. 5a). The equivalent plots for a fragmentation threshold of 0.7 exsolved gas volume fraction are shown in Supplementary Fig. S1.

Varying dome height introduces a step-like pattern to the eruption rate (Fig. 5c). This steep change in eruption rate occurs due to a transition in eruption style (effusive-explosive). In this case, compared to changing temperature (Fig. 5a) or magma chamber overpressure (Fig. 5b), a transition to explosive eruptions (fragmentation) has a much more pronounced effect on mass flow rate (Fig. 5c). Varying initial water mass fraction and initial crystal volume fraction has a relatively minor effect. For runs with no dome (upper surface, Fig. 5c), fragmentation occurs for all but the most viscous initial parameters (lower right, Fig. 5c; initial crystal volume fraction 0.48–0.5 and initial water mass fraction 0.03–0.036). As dome height increases (middle and bottom surfaces, Fig. 5c), the initial parameters resulting in fragmentation move towards the upper left in Fig. 5c (decreasing initial crystal volume fraction, increasing initial water mass fraction), representing less viscous magmas. This trend shows how larger domes (i.e. greater pressures at the vent) are required to suppress fragmentation as magma viscosity decreases (i.e. magma with lower crystal fractions and more volatiles).

The effusive-explosive regime diagrams in Fig. 6 highlight the critical conditions where fragmentation occurs over the standard range (Table 1; Fig. 2). In each of these panels the effusive regime is located in the lower right and the explosive regime is in the upper left. The black dots in the plot represent pairs of values for initial crystal volume fraction (x-axis) and initial water mass fraction (y-axis) for which multiple simulations have been performed by varying the third investigated parameter. The lines in each diagram are the fragmentation thresholds for the labeled value of the third parameter. At a temperature of 850 °C, for example, most runs in Fig. 6a are effusive, whereas for 950 °C, most runs are explosive. The space between fragmentation threshold lines represents the 'strength' of the third parameter in controlling fragmentation conditions, with greater spacing indicating greater effect. The equivalent plots for a fragmentation threshold of 0.7 exsolved gas volume fraction are in Supplementary Material.

In Fig. 6, we highlight fragmentation thresholds where small changes in initial parameter values, or unsteady processes or heterogeneities during ascent not captured by this model, can result in a transition in eruption style. For example, along the fragmentation threshold line for a magma temperature of 950 °C (Fig. 6a), a change of either 0.02 initial crystal volume fraction (between 0.46 and 0.44) or 0.002 initial water mass fraction (between 0.036 and 0.038) will result in a transition between effusive and explosive regimes (arrows, Fig. 6a). For a temperature of 850 °C, the critical values shift, for example, to 0.32–0.34 initial crystal volume fraction and 0.04–0.042 initial water mass fraction, showing the significance of temperature on

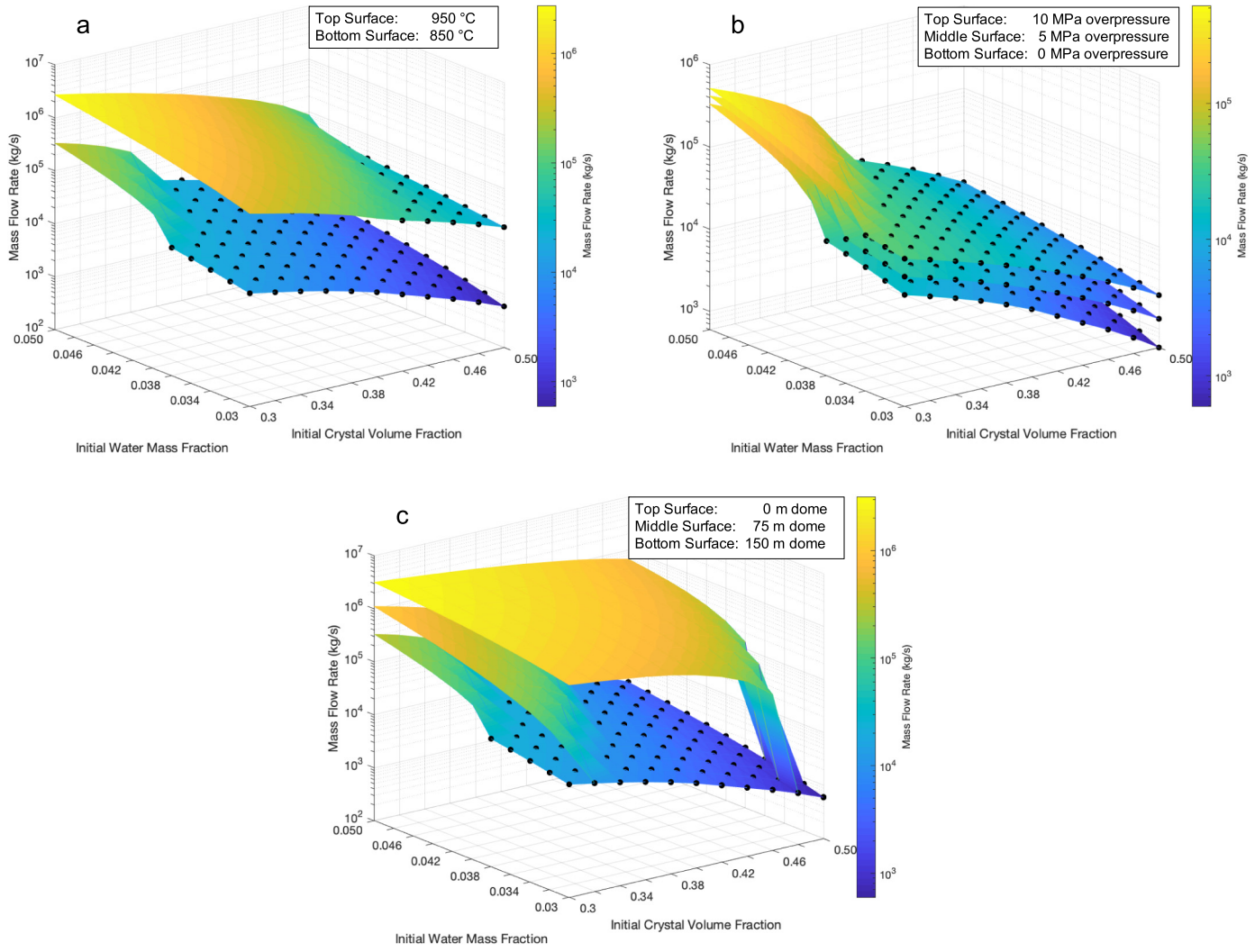

Fig. 5. Effects of multiple parameters on mass flow rate. Sets of three different parameters are compared to show the effect on mass flow rate of initial water mass fraction, initial crystal volume fraction, and (a) temperature, (b) magma chamber overpressure, and (c) dome height. Each surface represents the mass flow rate for each value of the third parameter. Each intersection of lines on the surface grid is a model run. Grid intersections with a black dot indicate that a run was effusive. The space between each surface shows the effect on the mass flow rate of changing the third parameter value, where more space between surfaces represents a greater effect. The greatest variations in mass flow rate occur when the combination of the three parameters controlling viscosity are changed (shown in a), while dome height (c) shows a sharp increase in mass flow rate at the critical value for fragmentation and a slower, steady rate of change for non-critical conditions. For the range represented here, the effect of overpressure (b) is minimal compared to the effects of water and crystal content.

fragmentation (Fig. 6a). We reiterate, for the range of initial water and crystal contents explored here, the explosive regime dominates at 950 °C, whereas the effusive regime dominates at 850 °C.

Fig. 6b again shows the relatively minor effect of magma chamber overpressure on fragmentation compared to other parameters, although increasing overpressure gently moves the system towards explosive activity. Under the right conditions (0.34 initial crystal volume fraction and 0.044 initial water mass fraction, shown as a star in Fig. 6b), an increase in overpressure of just a few MPa results in explosive eruption. However, for other conditions (0.34 initial crystal volume fraction and 0.04 initial water mass fraction, shown as a diamond in Fig. 6b) an increase from 0 to 10 MPa chamber overpressure will not cause fragmentation, while a decrease in initial crystal volume fraction of just 0.04 from the same position (from 0.34 to 0.3) will result in an explosive eruption, even for 0 MPa overpressure (thick arrow, Fig. 6b).

We acknowledge that the specific interpretations of transitions in eruption style are heavily influenced by model simplifications and chosen constants, especially the fragmentation model and threshold. We also recognize that natural systems are dynamic and contain heterogeneities at many scales and thus are not restricted to the same absolute distinctions as a numerical model. However, our model results allow an exploration of the effusive-explosive transition in order to highlight the relative role of different parameters in controlling eruptive regime; the suite of runs presented here suggest that for some conditions (called, 'critical conditions'), small changes in key parameters can abruptly shift eruption style, whereas for other conditions (away from fragmentation thresholds), even large changes in those same parameters will not change eruption style or eruption rate in a significant way.

3.2. Application to Merapi 2010

For the Merapi-specific case we fix the conduit length to 2000 m (Ratdomopurbo and Poupinet, 2000), and country rock density to 2600 kg m^{-3} (for a carbonate bedrock). We then vary the initial water mass fraction over a range of 0.04–0.06 (Costa et al., 2013), the initial crystal volume fraction over a range of 0.3–0.5 (Hammer et al., 2000), the temperature over a range of 950 °C – 1000 °C (Costa et al., 2013), the dome height over a range of 0–130 m (Pallister et al., 2013), the magma chamber overpressure over a range of 0–10 MPa (Carr et al.,

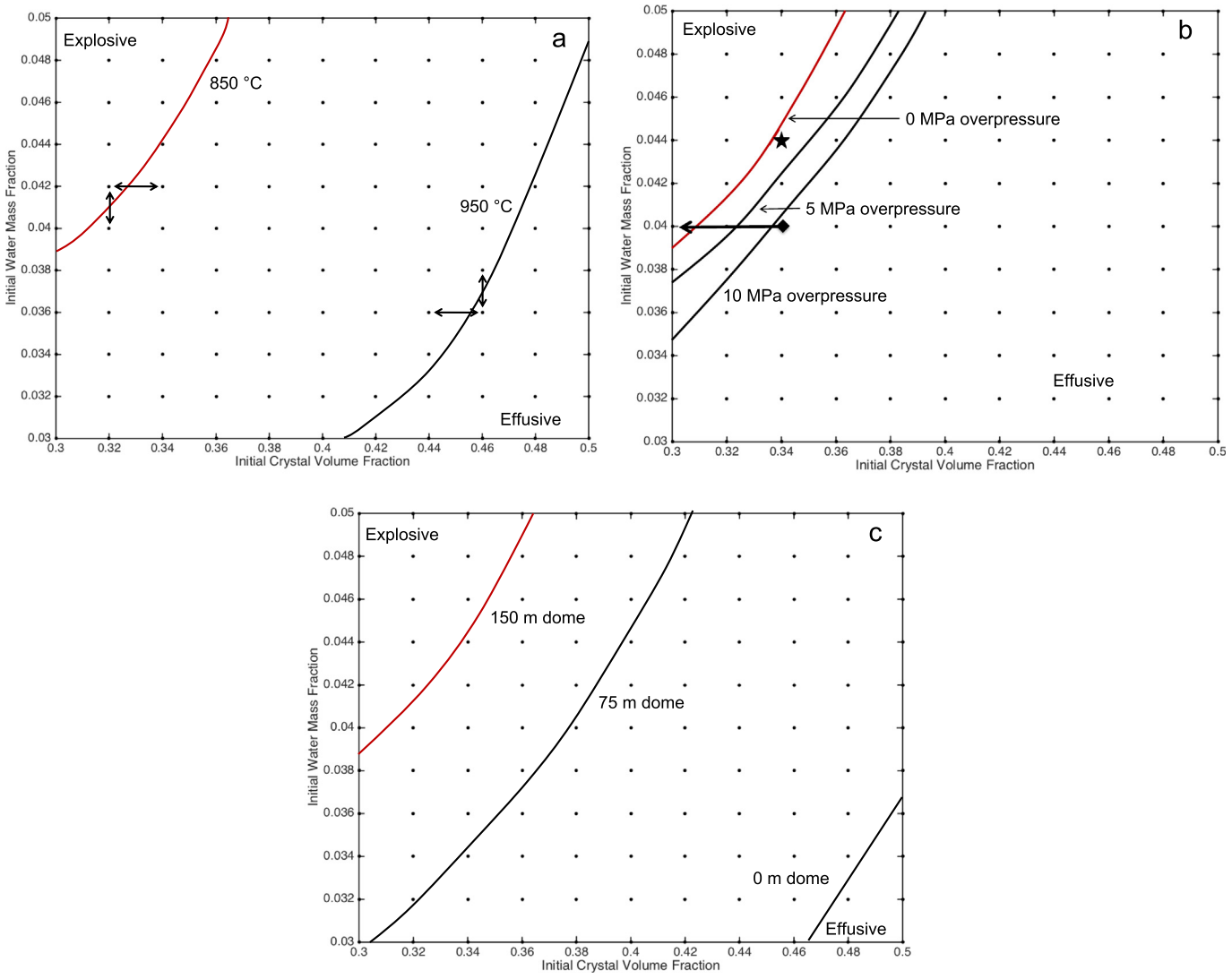

Fig. 6. Effects of multiple parameters on fragmentation. We show fragmentation as a phase boundary at conditions comparing 3 different variables: a) initial water mass fraction, initial crystal volume fraction, and temperature; b) initial water mass fraction, initial crystal volume fraction, and magma chamber overpressure; c) initial water mass fraction, initial crystal volume fraction, and dome height. The black dots represent parameter values used in the model runs. For example, each black dot in (a) represents two runs: one for each of the two temperatures, with values of initial crystal volume fraction and initial water mass fraction corresponding to the plotted location. Effusive conditions are towards the lower right and explosive conditions are towards the upper left. The fragmentation threshold is a solid line labeled by the value of the third parameter. A red line represents the fragmentation threshold for the 'standard' value of the third parameter and is thus in the same location in each of (a), (b), and (c). For the labeled third parameter value, effusive conditions will occur for water and crystal content values below the curve, and explosive conditions will occur for water and crystal content values above the curve. The arrows (a) show how small changes in initial crystal volume fraction or initial water mass fraction can result in crossing the fragmentation threshold line for a temperature of 950 °C. A larger separation of the fragmentation lines indicates a greater effect on fragmentation by the third parameter. (For interpretation of the references to colour in this figure legend, the reader is referred to the web version of this article.)

2018), and the lateral permeability exponent between −12 and −14 (Jaupart and Allègre, 1991).

As in Carr et al. (2018), we account for the potential effect of bedrock-derived CO_2 by varying the solubility coefficient σ, in the equation for the equilibrium dissolved volatile fraction, $x_d^{eq} = \sigma\sqrt{p/\overline{p}}$ (Sparks, 1978), where $\sigma = 4.11 \times 10^{-6}$ is the H_2O solubility coefficient, p is pressure [Pa], and $\overline{p}$ is a reference pressure, equal to 1 Pa (to make the equation dimensionally consistent). We apply the model of Papale et al. (2006) using Merapi magma compositions from Hammer et al. (2000) and Innocenti et al. (2013) to determine the relationship between the solubility coefficient and ppm of added CO_2. We run the solubility model for pressures from 0 MPa to 100 Mpa and vary the CO_2 content. We best fit the trend in the form of $x_d^{eq} = \sigma\sqrt{p/\overline{p}}$ (Sparks, 1978) for σ values over a range of 3.11×10^{-6} to 4.11×10^{-6}. We then use the corresponding changes in the exsolved volatile phase along with the model of Blake (1984) to calculate a range of possible overpressures generated in the 2 km-deep magma storage zone due to volatile oversaturation.

We select the runs that best describe the observed activity at Merapi (Runs 1–9, Table 1) from this set of parameters and use these results to assess the processes responsible for the documented 2010 eruptive activity, paying particular attention to rapid changes in eruption rate or style.

Using parameter values from previous studies on Merapi (Table 1), the conduit model accurately reproduces the mass and volume flow rates observed during both explosive and effusive phases of the 2010 eruption (Runs 1–9, Table 1). Run 1 (Table 1) represents the 26 October explosive initiation of the eruption. For an initial water mass fraction of 0.04 (Costa et al. (2013), initial crystal volume fraction of 0.44, and temperature of 970 °C, the magma fragments and erupts explosively with a mass flow rate of 1.4×10^6 kg s^{-1}, despite the initial confining pressure of the 50 m dome remaining from the 2006 eruption (Ratdomopurbo et al., 2013). The exceptionally high extrusion rates immediately

following the 26 October explosive phase rapidly built a new lava dome at a documented volume flow rate of approximately 25 $m^3 s^{-1}$ (Pallister et al., 2013). We model these conditions (Run 2, Table 1), achieving an extrusion rate of 28 $m^3 s^{-1}$ by using a dome height of 130 m and the same initial water mass fraction, initial crystal volume fraction, and temperature as Run 1. Note that Runs 2–9 (Table 1) employ a conduit wall rock permeability of 4.8×10^{-12}, an increase from the value of 4.8×10^{-14} used in Run 1 and for the 2006 effusive eruption (Table 1). We suggest the possibility that fracturing of the conduit walls during the initial explosive phase on 26 October 2010 caused an increase in conduit wall-rock permeability.

Following the approach adopted in the previous section, we explore the effects of parameters on eruption style by varying individual values from a standard (effusive) condition, here represented by Run 2 (Table 1). This comparison suggests that the Merapi system was near critical conditions during the 2010 eruption, where small perturbations of the system due to heterogeneous or changing parameter values or unsteady processes could result in fragmentation and a transition from an effusive to explosive eruption, and back again. For example, an explosive phase is initiated in the model under conditions otherwise identical to Run 2 by increasing the initial water mass fraction by just 0.001, from 0.040 to 0.041 (Run 3, Table 1). Similarly, a decrease in dome height of only 10 m, from 130 m to 120 m, a decrease in the wall-rock permeability, from 4.8×10^{-12} to 4.8×10^{-14}, or an increase in magma chamber overpressure, from 0 to 3 MPa, also result in an explosive eruption (Runs 4–6, Table 1) and mass flow rates of $1.6–2.1 \times 10^5$ kg s^{-1}. A decrease in the water solubility coefficient σ to 3.61×10^{-6}, corresponding to the addition of ~4000 ppm CO_2 (Papale et al., 2006), causes overpressure to build in the storage region as the bubble volume fraction increases. As overpressure increases from 0 to 5 MPa, extrusion rate increases from 20.7 to 34.0 $m^3 s^{-1}$. An explosive eruption occurs when overpressure reaches 6 MPa (Run 7, Table 1). Following the model of Blake (1984), overpressures of 0–10 MPa can be expected to occur due to the addition of 4000 ppm CO_2 to <1 vol% of the magma in the storage region at a depth of 2 km.

These small variations in initial parameters in the conduit model demonstrate the high-sensitivity of the effusive-explosive transition to the parameter conditions of Runs 2–7 (Table 1), where different eruption styles and mass flow rates are possible for very small changes in initial conditions. These model results suggest that the conditions in the Merapi system may have been near critical conditions in 2010 and that small parameter changes may have feasibly led to abrupt changes in eruption style, similar to those observed and documented.

Runs 3–7 (Table 1) demonstrate that several kinds of changes may have triggered the 4–5 November climactic explosive phase of the eruption, which we model explicitly in Runs 8 & 9 (Table 1). Assuming no dome conditions (a reasonable assumption because the initiation of the explosive phase destroyed the lava dome), maximum modeled mass flow rates are $3.5–5.3 \times 10^6$ kg s^{-1} for the range of volatile contents measured in samples from the eruption by Costa et al. (2013) (Runs 8 & 9, Table 1). The modeled mass flow rates were $1.4–5.3 \times 10^6$ kg s^{-1} for the three largest explosive phases (Runs 1, 8, & 9, Table 1) and are within the range of $10^6–10^7$ kg s^{-1} that are expected to produce eruption plumes between 12 and 17 km in height (Wilson and Walker, 1987; Mastin et al., 2009; Pallister et al., 2013).

4. Discussion

The broad range of model results for multiple parameters presented here allows us to comment on two types of effusive-explosive transitions: those that occur between distinct eruption events, and those that occur within a single eruption episode. Furthermore, we are able to apply these concepts to explain effusive-explosive transitions at Merapi volcano, both between the 2006 and 2010 eruptions and during the 2010 eruption.

4.1. Transitions between distinct eruptions

Parameters affecting magma viscosity have the greatest influence on whether or not an eruption is effusive or explosive, and consequently, exert the greatest influence on the resulting mass flow rate (Fig. 3). A transition in eruption style can occur if the viscosity of the magma changes between eruptions (Fig. 4). This can be achieved without changing the composition of the magma, but instead by altering the water mass fraction, crystal volume fraction, and/or temperature of the magma entering the conduit through mixing with new magma of the same composition ascending into the system. The new magma may be hotter, higher in volatile content, and lower in crystal content compared to a magma residing in a shallow storage system (Ruprecht and Bachmann, 2010). If this newly mixed magma does not stall during ascent, its lower viscosity will favor explosive eruption compared to the pre-existing magma in the shallow storage system.

Conversely, if magma entering or remaining in a shallow storage region following an explosive eruption has time to cool, degas, and/or crystallize prior to rising towards the vent, it will favor effusive eruption largely due to its higher viscosity and relatively degassed state. This is likely the case for dome-forming eruptions that follow in the months to years after large explosive eruptions, such as at Mount St. Helens in Washington, USA (Fink et al., 1990) and Santiaguito Volcano in Guatemala (Anderson et al., 1995).

4.2. Transitions during eruption episodes

For rapid transitions between explosive and effusive activity to occur within a single eruption episode, the volcanic system must be at critical conditions, where small perturbations of the system can cause the rising magma to cross the fragmentation threshold (Fig. 6). This concept has been described previously for scenarios involving small variations in magma chamber overpressure (Woods and Koyaguchi, 1994), viscosity (Kozono and Koyaguchi, 2012), and dome height (Melnik and Sparks, 1999; Woods and Koyaguchi, 1994), as well as short periods of permeable gas loss (Kozono and Koyaguchi, 2012; Degruyter et al., 2012). When at critical conditions (Fig. 6), small variations in initial water mass fraction or initial crystal volume fraction can cause eruption style to change. The variations may be sufficiently small to be attributed to natural small- to medium-scale heterogeneities in a magma chamber. If values of initial water mass fraction and initial crystal volume fraction remain constant, critical values of temperature, dome height, and magma chamber overpressure also exist, such that sudden changes in eruption style may occur with small changes in these parameters (Figs. 3, 5 & 6).

Explosive eruptions lacking an effusive phase and sustained effusive eruptions are likely examples of systems in which the magma is not near critical conditions. Because small variations in parameters will not change the eruption type, the eruption style is stable and will continue until reservoir pressure decreases and the supply of magma diminishes - rapidly over hours to days for explosive eruptions or slowly over months or years for effusive eruptions. The 2014 eruption of Kelud, which did not produce any effusive activity before or after the February 14 explosion (Global Volcanism Program, 2014), may be an example of eruption of a finite, homogeneous batch of magma that was sitting in a 'stable explosive state'. Analogously, the l990–1995 eruption of Unzen Volcano (Japan) (Nakada et al., 1999) may be an example of the eruption of magma sitting in a 'stable effusive state'.

4.3. Transitions at Merapi in 2010

Our model results are consistent with observations of the 2010 Merapi eruption (Surono et al., 2012; Costa et al., 2013; Pallister et al., 2013; Preece et al., 2016). The volume flow rate of 28.1 $m^3 s^{-1}$ that we calculate in Run 2 (Table 1) is within the range of 25–35 $m^3 s^{-1}$ described by Pallister et al. (2013). The maximum mass flow rate of

5.3×10^6 kg s^{-1} (Run 9, Table 1) is within the range of 10^6–10^7 kg s^{-1} expected for an eruption generating a 17 km high plume, similar to that generated on 4–5 November 2010 (Wilson and Walker, 1987; Mastin et al., 2009; Pallister et al., 2013). From the 2006 eruption to the 2010 eruption, our model results suggest that there may have been increase in water mass fraction from 0.025 to 0.04, a decrease in crystal volume fraction from 0.5 to 0.44, and a temperature increase from 950 to 970 °C (Table 1) in the shallow storage region at 2 km depth. These changes can be explained by a rising batch of magma in 2010 that mixed with a cooler, more crystalline, degassed magma remaining from the 2006 eruption (Table 1), and then, due to the volume and ascent rate of the rising magma batch, erupted without having time to cool, crystalize, and/or degas (Fig. 7a). Rapid ascent of the magma created conditions more favorable for explosive eruptions and high extrusion rates during effusive activity. This explanation for the cause of the more violent 2010 eruption is consistent with several previous studies that used different lines of inquiry. For example, the conclusions of Surono et al. (2012), based on monitoring and petrologic observations, suggest a similar cause for the change in eruption style. From petrologic analysis, Preece et al. (2016) conclude that the cause of the transition from effusive eruption in 2006 to explosive eruption in 2010 was driven by an increase in magma flux from depth and subsequent higher ascent rates. Costa et al. (2013) explain that while the magma prior to the 2006 eruption had time to crystallize and degas in a shallow storage region, leading to an effusive eruption (and the model input parameters in Table 1 and Carr et al., 2018), the volume of magma entering the system in 2010 overwhelmed the shallow storage region, which limited the degassing and crystallization that could occur, and resulted in an explosive eruption.

We propose an additional idea here: the rising batch of new magma led to critical conditions in the Merapi shallow storage system in 2010, resulting in rapid fluctuations in eruption style with alternating effusive – explosive behavior (Fig. 7b & c). Small variations in either initial water mass fraction or dome height result in a transition from effusive to explosive eruption (Runs 2–4, Table 1; Fig. 7b & c)- variations that can reasonably be explained by eruption from a heterogeneous magma chamber (Fig. 7b), as suggested by Surono et al. (2012). Preece et al. (2016) attribute the effusive-explosive transitions to closed-system degassing conditions that developed during dome extrusion and allowed pressure to build in the shallow conduit (Fig. 7b & c). We show that for this to be a feasible explanation, a decrease in the wall-rock permeability of two orders of magnitude is required, from 4.8×10^{-12} to 4.8×10^{-14}.

Given the frequency of block and ash flows during this and other Merapi eruptions, dome collapse is also a reasonable explanation for the initiation of explosive activity (Run 4, Table 1; Fig. 7c). However, we note that no descriptions of the eruption mention dome collapses preceding the explosive phases in 2010, and in the case of the October 26 explosion, sources specifically mention the lack of any dome instability or collapses prior to this event (Surono et al., 2012; Pallister et al., 2013).

A storage zone overpressure increase of 3 MPa can also trigger an explosive eruption (Run 5, Table 1; Fig. 7c). However, regional deformation at Merapi prior to the 2010 eruption was not observed by InSAR (Chaussard and Amelung, 2012; Saepuloh et al., 2013), and only one electronic distance measurement (EDM) baseline showed significant change (Saepuloh et al., 2013). We conclude that any overpressure that developed was localized, did not cause ground deformation at spatial or temporal scales observable by InSAR, and that the other mechanisms described here [heterogeneous water content, variable shallow conduit degassing, addition of CO_2] are more likely triggers of the transitions in eruption style relative to overpressure caused by increased magma flux affecting the entire shallow storage region.

The addition of CO_2 to the magma through decarbonation of the carbonate bedrock can affect eruptive style by reducing the solubility of water in the magma, causing exsolution of volatiles and increasing bubble volume fraction and overpressure in the shallow storage zone. Deegan et al. (2010), Troll et al. (2012), and Carr et al. (2018) show that activity at Merapi in 2006 was likely affected by this process, and Costa et al. (2013) suggest that decarbonation is likely to have been increased in 2010 due to the increased temperature and volume of the magma in the shallow storage zone. Our results agree, and indicate that given the critical conditions likely to have existed during the 2010 eruption, the addition of approximately 4000 ppm CO_2 to <1 vol % of magma in the shallow storage zone is needed to trigger an explosive eruption. We also emphasize here that the overpressure that developed as a result of decarbonation was likely to have been short-lived and to have occurred over a small volume, in contrast to overpressure that would develop due to greater magma flux into the storage region. We offer this as an explanation for why no significant regional ground deformation was observed by InSAR during the eruption (Chaussard and Amelung, 2012; Saepuloh et al., 2013) and only one ground-based EDM baseline recorded significant change (Saepuloh et al., 2013). Overpressure associated with decarbonation may have affected only a small portion of the shallow storage zone, focusing deformation over a small area and not generating sufficient deformation to be detected by InSAR.

Our steady-state numerical model is unable to fully capture the transition from explosive back to effusive activity. All model runs where the dome height was set to 0 m- representing the explosion destroying the dome- remain explosive. We thus attribute the explosive to effusive transition to unsteady shallow conduit processes, most likely related to either separation of the gas and melt phases of the magma via

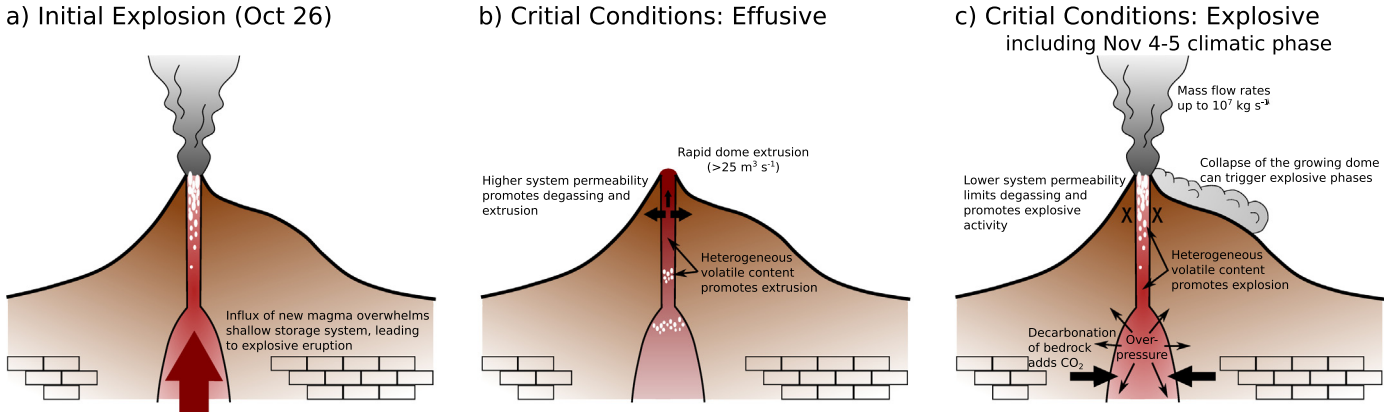

Fig. 7. Eruptive conditions at Merapi in 2010. The 2010 eruption began (a) when new magma entered and overwhelmed the shallow Merapi storage system, leading to an explosive eruption. The influx of new magma also moved the system into critical conditions, where small changes in certain parameters [volatile content, dome height, magma chamber overpressure, wall-rock permeability, and H_2O solubility due to addition of CO_2 from the carbonate bedrock] could cause rapid transitions between effusive (b) and explosive (c) activity.

permeable pathways and enhanced open-system degassing, as suggested by Preece et al. (2016), or an increasing conduit diameter, as described by Aravenna et al. (2017). Enhanced open-system degassing may be favored during the waning stages of explosive phases due to depletion of overpressure as high mass eruption rates empty the shallow storage region.

5. Conclusions

We use a numerical model of magma ascent in a volcanic conduit to investigate effusive-explosive eruption transitions in silicic volcanic systems. In general, the parameters controlling the viscosity of the magma – initial water mass fraction, initial crystal volume fraction, and temperature – exert the greatest control on the mass flow rate and whether or not an explosive eruption occurs, with low viscosities favoring high ascent rates and therefore explosive eruption. We also compare multiple parameters against one another and identify critical conditions for different sets of parameters under which small perturbations within the system may cause a change in eruption style. Initial water mass fraction and initial crystal volume fraction are key parameters in defining conditions necessary for a system to be in a critical condition.

Our results support the suggestion that the transition at Merapi Volcano from effusive eruption in 2006 to explosive eruption in 2010 was caused by the fast ascent of a volatile-rich batch of magma that was too large to be accommodated in the shallow storage system (Costa et al., 2013) (Fig. 7a). We add that the new batch of magma may have pushed the Merapi system into critical conditions, leading to multiple transitions over a short period during the 2010 eruption (Fig. 7b & c). These results and the idea of critical conditions at Merapi are consistent with mechanisms for effusive-explosive transitions suggested in previous work, such as heterogeneities in water mass fraction (Surono et al., 2012) and variable degassing conditions in the shallow conduit (Preece et al., 2016). We also demonstrate that the addition of CO_2 to the magma from decarbonation of bedrock- a process that has been previously identified at Merapi- can significantly affect water solubility and thus the bubble volume fraction, and we offer this as an additional feasible mechanism for transition between effusive and explosive activity during the 2010 eruption.

Supplementary data to this article can be found online at https://doi.org/10.1016/j.jvolgeores.2019.106767.

CRediT authorship contribution statement

Brett B. Carr: Conceptualization, Methodology, Investigation, Writing - original draft, Writing - review & editing, Visualization. **Amanda B. Clarke:** Conceptualization, Methodology, Writing - review & editing, Supervision. **Mattia de' Michieli Vitturi:** Methodology, Software, Writing - review & editing.

Declaration of competing interest

The authors declare that they have no known competing financial interests or personal relationships that could have appeared to influence the work reported in this paper.

Acknowledgements

Author BC was supported in part by summer Ph.D. student research fellowships awarded by the School of Earth and Space Exploration and funded by a Graduate College University Block Grant at Arizona State University.

References

Adams, B.M., Bauman, L.E., Bohnhoff, W.J., Dalbey, K.R., Ebeida, M.S., Eddy, J.P., Eldred, M.S., Hough, P.D., Hu, K.T., Jakeman, J.D., Stephens, J.A., Swiler, L.P., Vigil, D.M., Wildey, T.M., July 2014. Dakota, A Multilevel Parallel Object-Oriented Framework for Design Optimization, Parameter Estimation, Uncertainty Quantification, and Sensitivity Analysis: Version 6.0 User's Manual. Sandia Technical Report SAND2014-4633. (Updated November 2015 (Version 6.3).

Anderson, S.W., Fink, J.H., Rose, W.I., 1995. Mount St. Helens and Santiaguito lava domes: the effect of short-term eruption rate on surface texture and degassing processes. J. Volcanol. Geotherm. Res. 69, 105–116. https://doi.org/10.1016/0377-0273(95)00022-4.

Aravenna, Á., de' Michieli Vitturi, M., Cioni, R., Neri, A., 2017. Stability of volcanic conduits during explosive eruptions. J. Volcanol. Geotherm. Res. 339, 52–62. https://doi.org/10.1016/j.jvolgeores.2017.05.003.

Blake, S., 1984. Volatile oversaturation during the evolution of silicic magma chambers as an eruption trigger. J. Volcanol. Geotherm. Res. 89, 8237–8244. https://doi.org/10.1029/JB089iB10p08237.

Calder, E.S., Luckett, R., Sparks, R.S.J., Voight, B., 2002. Mechanisms of lava dome instability and generation of rockfalls and pyroclastic flows at Soufrière Hills Volcano, Montserrat. In: Druitt, T.H., Kokelaar, B.P. (Eds.), The Eruption of Soufrière Hills Volcano, Montserrat, from 1995 to 1999. Geol. Soc. Lond. Mem 21, pp. 173–190. https://doi.org/10.1144/GSL.MEM.2002.021.01.08.

Carr, B.B., Clarke, A.B., de' Michieli Vitturi, M., 2018. Earthquake induced variations in extrusion rate: a numerical modeling approach to the 2006 eruption of Merapi Volcano (Indonesia). Earth Planet. Sci. Lett. 482, 377–387. https://doi.org/10.1016/j.epsl.2017.11.019.

Charbonnier, S.J., Gertisser, R., 2008. Field observations and surface characteristics of pristine block-and-ash flow deposits from the 2006 eruption of Merapi Volcano, Java, Indonesia. J. Volcanol. Geotherm. Res. 177, 971–982. https://doi.org/10.1016/j.jvolgeores.2008.07.008.

Charbonnier, S.J., Germa, A., Connor, C.B., Gertisser, R., Preece, K., Komorowski, J.C., Lavigne, F., Dixon, T., Connor, L., 2013. Evaluation of the impact of the 2010 pyroclastic density currents at Merapi volcano from high-resolution satellite imagery, field investigations and numerical simulations. J. Volcanol. Geotherm. Res. 261, 295–315. https://doi.org/10.1016/j.jvolgeores.2012.12.021.

Chaussard, E., Amelung, F., 2012. Precursory inflation of shallow magma reservoirs at west Sunda volcanoes detected by InSAR. Geophys. Res. Lett. 39, L21311. https://doi.org/10.1029/2012GL053817.

Clarke, A.B., Stephens, S., Teasdale, R., Sparks, R.S.J., Diller, K., 2007. Petrologic constraints on the decompression history of magma prior to Vulcanian explosions at the Soufriere Hills volcano, Montserrat. J. Volcanol. Geotherm. Res. 161, 261–274. https://doi.org/10.1016/j.jvolgeores.2006.11.007.

Costa, A., 2005. Viscosity of high crystal content melts: dependence on solid fraction. Geophys. Res. Lett. 32, L22308. https://doi.org/10.1029/2005GL024303.

Costa, F., Andreastuti, S., de Maisonneuve, C.B., Pallister, J.S., 2013. Petrological insights into the storage conditions, and magmatic processes that yielded the centennial 2010 Merapi explosive eruption. J. Volcanol. Geotherm. Res. 261, 209–235. https://doi.org/10.1016/j.jvolgeores.2012.12.025.

de' Michieli Vitturi, M., Clarke, A.B., Neri, A., Voight, B., 2011. Assessing the influence of disequilibrium crystallization and degassing during magma ascent in effusive and explosive eruptions. American Geophysical Union, Fall Meeting (abstract #V23H-05).

de' Michieli Vitturi, M., Clarke, A.B., Neri, A., Voight, B., 2013. Extrusion cycles during dome-building eruptions. Earth Planet. Sci. Lett. 371-372, 37–48. https://doi.org/10.1016/j.epsl.2013.03.037.

Deegan, F.M., Troll, V.R., Freda, C., Misiti, V., Chadwick, J.P., McLeod, C.L., Davidson, J.P., 2010. Magma-carbonate interaction processes and associated CO_2 release at Merapi Volcano, Indonesia: insights from experimental petrology. J. Petrol. 51, 1027–1051. https://doi.org/10.1093/petrology/egq010.

Degruyter, W., Bachmann, O., Burgisser, A., Manga, M., 2012. The effects of outgassing on the transition between effusive and explosive silicic eruptions. Earth Planet. Sci. Lett. 349-350, 161–170. https://doi.org/10.1016/j.epsl.2012.06.056.

Diller, K., Clarke, A.B., Voight, B., Neri, A., 2006. Mechanisms of conduit plug formation: Implications for vulcanian explosions. Geophys. Res. Lett. 33, L20302. https://doi.org/10.1029/2006GL027391.

Eichelberger, J.C., Carrigan, C.R., Westrich, H.R., Price, R.H., 1986. Non-explosive silicic volcanism. Nature 323, 598–602. https://doi.org/10.1038/323598a0.

Fink, J.H., Malin, M.C., Anderson, S.W., 1990. Intrusive and extrusive growth of the Mount St Helens lava dome. Nature 348, 435–437. https://doi.org/10.1038/348435a0.

Gertisser, R., Charbonnier, S.J., Keller, J., Quidelleur, X., 2012. The geological evolution of Merapi volcano, Central Java, Indonesia. Bull. Volcanol. 74, 1213–1233. https://doi.org/10.1007/s00445-012-0591-3.

Global Volcanism Program, 2014. Report on Kelut (Indonesia). In: Wunderman, R (Ed.) Bulletin of the Global Volcanism Network, 39:2. Smithsonian Institution https://doi.org/10.5479/si.GVP.BGVN201402-263280.

Gonnermann, H.M., Manga, M., 2003. Explosive volcanism may not be an inevitable consequence of magma fragmentation. Nature 426, 432–435. https://doi.org/10.1038/nature02138.

Hammer, J.E., Cashman, K.V., Voight, B., 2000. Magmatic processes revealed by textural and compositional trends in Merapi dome lavas. J. Volcanol. Geotherm. Res. 100, 165–192. https://doi.org/10.1016/S0377-0273(00)00136-0.

Hess, K.-U., Dingwell, D.B., 1996. Viscosities of hydrous leucogranitic melts: a non-Arrhenian model. Am. Mineral. 81, 1297–1300. https://doi.org/10.2138/am-1996-9-1031.

Innocenti, S., del Marmol, M.-A., Voight, B., Andreastuti, S., Furman, T., 2013. Textural and mineral chemistry constraints on evolution of Merapi Volcano, Indonesia. J. Volcanol. Geotherm. Res. 261, 20–37. https://doi.org/10.1016/j.jvolgeores.2013.01.006.

Jaupart, C., Allègre, C.J., 1991. Gas content, eruption rate and instabilities of eruption regime in silicic volcanoes. Earth Planet. Sci. Lett. 102, 413–429. https://doi.org/10.1016/0012-821X(91)90032-D.

Komorowski, J.-C., Jenkins, S., Baxter, P.J., Picquout, A., Lavigne, F., Charbonnier, S.J., Gertisser, R., Preece, K., Cholik, N., Budi-Santoso, A., Surono, 2013. Paroxysmal dome

explosion during the Merapi 2010 eruption: processes and facies relationships of associated high-energy pyroclastic density currents. J. Volcanol. Geotherm. Res. 261, 260–294. https://doi.org/10.1016/j.jvolgeores.2013.01.007.
Kozono, T., Koyaguchi, T., 2012. Effects of gas escape and crystallization on the complexity of conduit flow dynamics during lava dome eruptions. J. Geophys. Res. 117, B08204. https://doi.org/10.1029/2012JB009343.
La Spina, G., Burton, M., de' Michieli Vitturi, M., 2015. Temperature evolution during magma ascent in basaltic effusive eruptions: a numerical application to Stromboli volcano. Earth Planet. Sci. Lett. 426, 89–100. https://doi.org/10.1016/j.epsl.2015.06.015.
La Spina, G., de' Michieli Vitturi, M., Clarke, A.B., 2017. Transient numerical model of magma ascent dynamics: application to the explosive eruptions at the Soufrière Hills Volcano. J. Volcanol. Geotherm. Res. 336, 118–139. https://doi.org/10.1016/j.jvolgeores.2017.02.013.
La Spina, G., Clarke, A.B., de' Michieli Vitturi, M., Burton, M., Allison, C.M., Roggensack, K., Alfano, F., 2019. Conduit dynamics of highly explosive basaltic eruptions: the 1085 CE Sunset Crater sub-Plinian events. J. Volcanol. Geotherm. Res. 387, 106658. https://doi.org/10.1016/j.jvolgeores.2019.08.001.
Llewellin, E.W., Manga, M., 2005. Bubble suspension rheology and implications for conduit flow. J. Volcanol. Geotherm. Res. 143, 205–217. https://doi.org/10.1016/j.jvolgeores.2004.09.018.
Mastin, L.G., 2002. Insights into volcanic conduit flow from an open-source numerical model. Geochem. Geophys. 3 (7). https://doi.org/10.1029/2001GC000192.
Mastin, L.G., Guffanti, M., Servranckx, R., Webley, P., Barsotti, S., Dean, K., Durant, A., Ewert, J.W., Neri, A., Rose, W.I., Schneider, D., Siebert, L., Stunder, B., Swanson, G., Tupper, A., Volentik, A., Waythomas, C.F., 2009. A multidisciplinary effort to assign realistic source parameters to models of volcanic ash-cloud transport and dispersion during eruptions. J. Volcanol. Geotherm. Res. 186, 10–21. https://doi.org/10.1016/j.jvolgeores.2009.01.008.
Melnik, O., Sparks, R.S.J., 1999. Nonlinear dynamics of lava dome extrusion. Nature 402, 37–41. https://doi.org/10.1038/46950.
Melnik, O., Sparks, R.S.J., 2002. Modelling of conduit flow dynamics during explosive activity at Soufrière Hills Volcano, Montserrat. In: Druitt, T.H., Kokelaar, B.P. (Eds.), The Eruption of Soufrière Hills Volcano, Montserrat, From 1995 to 1999. Geol. Soc. Lond. Mem 21, pp. 307–317. https://doi.org/10.1144/GSL.MEM.2002.021.01.07.
Nakada, S., Shimizu, H., Ohta, K., 1999. Overview of the 1990-1995 eruption at Unzen Volcano. J. Volcanol. Geotherm. Res. 89, 1–22. https://doi.org/10.1016/S0377-0273(98)00118-8.
Newhall, C.G., Self, S., 1982. The Volcanic Explosivity Index (VEI): an estimate of explosive magnitude for historical volcanism. J. Geophys. Res. 87, 1231–1238. https://doi.org/10.1029/JC087iC02p01231.
Newhall, C.G., Bronto, S., Alloway, B., Banks, N.G., Bahar, I., del Marmol, M.A., Hadisantono, R.D., Holcomb, R.T., McGeehin, J., Miksic, J.N., Rubin, M., Sayudi, S.D., Sukhyar, R., Andreastuti, S., Tilling, R.I., Trimble, D., Wirakusumah, A.D., 2000. 10,000 years of explosive eruptions of Merapi Volcano, Central Java: archaeological and modern implications. J. Volcanol. Geotherm. Res. 100, 9–50. https://doi.org/10.1016/S0012-821X(01)00443-5.
Pallister, J.S., Schneider, D.J., Griswold, J.P., Keeler, R.H., Burton, W.C., Noyles, C., Newhall, C.G., Ratdomopurbo, A., 2013. Merapi 2010 eruption- chronology and extrusion rates monitored with satellite radar and used in eruption forecasting. J. Volcanol. Geotherm. Res. 261, 144–152. https://doi.org/10.1016/j.jvolgeores.2012.07.012.
Papale, P., 1999. Strain-induced magma fragmentation in explosive eruptions. Nature 397, 425–428. https://doi.org/10.1038/17109.
Papale, P., Moretti, R., Barbato, D., 2006. The compositional dependence of the saturation surface of H_2O+CO_2 fluids in silicate melts. Chem. Geol. 229, 78–95. https://doi.org/10.1016/j.chemgeo.2006.01.013.
Preece, K., Gertisser, R., Barclay, J., Charbonnier, S.J., Komorowski, J.-C., Herd, R.A., 2016. Transitions between explosive and effusive phases during the cataclysmic 2010 eruption of Merapi volcano, Java, Indonesia. Bull. Volcanol. 78, 54. https://doi.org/10.1007/s00445-016-1046-z.
Ratdomopurbo, A., Poupinet, G., 2000. An overview of seismicity of Merapi volcano (Java, Indonesia), 1983-1994. J. Volcanol. Geotherm. Res. 100, 193–214. https://doi.org/10.1016/S0377-0273(00)00137-2.
Ratdomopurbo, A., Beauducel, F., Subandrio, J., Nandaka, I.G.M.A., Newhall, C.G., Suharna, Sayudi, Suparwaka, D.S., Sunarta, H., 2013. Overview of the 2006 eruption of Mt. Merapi. J. Volcanol. Geotherm. Res. 261, 87–97. https://doi.org/10.1016/j.jvolgeores.2013.03.019.
Romenski, E., Drikakis, D., Toro, E., 2010. Conservative models and numerical methods for compressible two-phase flow. J. Sci. Comput. 42, 68–95. https://doi.org/10.1007/s10915-009-9316-y.
Ruprecht, P., Bachmann, O., 2010. Pre-eruptive reheating during magma mixing at Quizapu volcano and the implications for the explosiveness of silicic arc volcanoes. Geology 38, 919–922. https://doi.org/10.1130/G31110.1.
Saepuloh, A., Urai, M., Aisyah, N., Sunarta, Widiwijayanti, C., Subandriyo, Jousset, P., 2013. Interpretation of ground surface changes prior to the 2010 large eruption of Merpai volcano using ALOS/PALSAR, ASTER TIR and gas emission data. J. Volcanol. Geotherm. Res. 261, 130–143. https://doi.org/10.1016/j.jvolgeores.2013.05.001.
Simkin, T., 1993. Terrestrial volcanism in space and time. Annu. Rev. Earth Planet. Sci. 21, 427–452. https://doi.org/10.1146/annurev.ea.21.050193.002235.
Siswowidjoyo, S., Suryo, I., Yokoyama, I., 1995. Magma eruption rates of Merapi volcano, Central Java, Indonesia during one century (1890-1992). Bull. Volcanol. 57, 111–116. https://doi.org/10.1007/BF00301401.
Sparks, R.S.J., 1978. The dynamics of bubble formation and growth in magmas: a review and analysis. J. Volcanol. Geotherm. Res. 3, 1–37. https://doi.org/10.1016/0377-0273(78)90002-1.
Surono, S., Jousset, P., Pallister, J., Boichu, M., Buongiorno, M.F., Budisantoso, A., Costa, F., Andreastuti, S., Prata, F., Schneider, D., Clarisse, L., Humaida, H., Sumarti, S., Bignami, C., Griswold, J., Carn, S., Oppenheimer, C., Lavigne, F., 2012. The 2010 explosive eruption of Javas Merapi volcano- a 100-year event. J. Volcanol. Geotherm. Res. 241–242, 121–135. https://doi.org/10.1016/j.jvolgeores.2012.06.018.
Troll, V.R., Hilton, D.R., Jolis, E.M., Chadwick, J.P., Blythe, L.S., Deegan, F.M., Schwarzkopf, L.M., Zimmer, M., 2012. Crustal CO_2 liberation during the 2006 eruption and earthquake events at Merapi volcano, Indonesia. Geophys. Res. Lett. 39, L11302. https://doi.org/10.1029/2012GL051307.
Voight, B., Davis, M.J., 2000. Emplacement temperatures of the November 22, 1994 nuée ardente deposits, Merapi Volcano, Java. J. Volcanol. Geotherm. Res. 100, 371–377. https://doi.org/10.1016/S0377-0273(00)00146-3.
Voight, B., Constantine, E.K., Siswowidjoyo, S., Torley, R., 2000. Historical eruptions of Merapi Volcano, Central Java, Indonesia, 1768-1998. J. Volcanol. Geotherm. Res. 100, 69–138. https://doi.org/10.1016/S0377-0273(00)00134-7.
Wilson, L., Walker, G.P.L., 1987. Explosive volcanic eruptions - VI. Ejecta dispersal in plinian eruptions: the control of eruption conditions and atmospheric properties. Geophys. J. Int. 89, 657–679. https://doi.org/10.1111/j.1365-246X.1987.tb05186.x.
Wilson, L., Sparks, R.S.J., Walker, G.P.L., 1980. Explosive volcanic eruptions - IV. The control of magma properties and conduit geometry on eruption column behaviour. Geophys. J. Int. 63, 117–148. https://doi.org/10.1111/j.1365-246X.1980.tb02613.x.
Wolpert, R.L., Ogburn, S.E., Calder, E.S., 2016. The longevity of lava dome eruptions. J. Geophys. Res. Solid Earth 121. https://doi.org/10.1002/2015JB012435.
Woods, A.W., Koyaguchi, T., 1994. Transitions between explosive and effusive eruptions of silicic magmas. Nature 370, 641–644. https://doi.org/10.1038/370641a0.
Zhang, Y., 1999. A criterion for the fragmentation of bubbly magma based on brittle failure theory. Nature 402, 648–650. https://doi.org/10.1038/45210.